Veget Hist Archaeobot (2014) 23:527–542
DOI 10.1007/s00334-013-0420-4

ORIGINAL ARTICLE

Inter-proxy evidence for the development of the Amazonian mangroves during the Holocene

Marlon C. França · Mariah I. Francisquini · Marcelo C. L. Cohen · Luiz C. R. Pessenda

Received: 4 February 2013 / Accepted: 4 October 2013 / Published online: 15 October 2013

Abstract The dynamics of mangrove forest on the island of Marajó (Ilha de Marajó) at the mouth of the river Amazon during the past ~7,500 cal. B.P. were studied using multiple proxies, including sedimentary facies, pollen, $\delta^{13}C$, $\delta^{15}N$ and C/N ratio, related to 15 sediment samples by ^{14}C dating. The results allow us to propose a scheme of palaeogeographical development, with changes in vegetation, hydrology and organic matter dynamics. Today, the interior of the island is occupied by *várzea* freshwater herbaceous vegetation, but during the early to middle Holocene, mangroves with accumulations of estuarine organic matter colonized the tidal mud flats. This spread of mangroves was caused by post-glacial sea-level rise, which combined with tectonic subsidence, produced a marine transgression. It is likely that the relatively greater marine influence at the studied area was favoured by reduced discharge from the river Amazon, which was itself caused by a dry period that occurred during the early and mid Holocene. During the late Holocene, there was a reduction of mangrove vegetation and the contribution of freshwater organic matter to the area was higher than during the early and mid Holocene. This suggests a decrease in marine influence during the late Holocene which led to a gradual migration of mangrove vegetation from the central region to the northeastern littoral zone of the island, and, consequently, its isolation since at least ~1,150 cal. B.P. This was probably a result of lower tidal water salinity caused by a wet period that resulted in greater river discharge during the late Holocene. This work details the contraction of mangrove forest from the northeastern part of the island of Marajó under the influence of Amazon climatic changes, chronologically and spatially. This allows us to propose a model of successive phases of sediment accumulation and vegetation change, according to the marine-freshwater influence gradient. As demonstrated by this work, the use of a combination of proxies is efficient for establishing a relationship between the changes in estuarine salinity gradient and depositional environment/vegetation.

Keywords Amazon coastal area · Holocene · Isotopes · Sea-level · Vegetation · Climate change

Communicated by P. I. Moreno M.

Electronic supplementary material The online version of this article (doi:10.1007/s00334-013-0420-4) contains supplementary material, which is available to authorized users.

M. C. França · M. C. L. Cohen (✉)
Post-Graduate Program of Geology and Geochemistry, Laboratory of Coastal Dynamics, Federal University of Pará, Av. Perimentral 2651, Terra Firme, Belém, PA CEP 66077-530, Brazil
e-mail: mcohen@ufpa.br

M. C. França
Federal Institute of Pará, Av. Almirante Barroso, 1155, Marco, Belém, PA CEP 66090-020, Brazil

M. I. Francisquini · L. C. R. Pessenda
14C Laboratory, University of São Paulo, Avenida Centenário 303, Piracicaba, São Paulo 13400-000, Brazil

M. C. L. Cohen
Faculty of Oceanography, Federal University of Pará, Rua Augusto Corrêa, n 1, Guama, Belém, PA CEP 66075-110, Brazil

Introduction

Mangrove distributions are considered to be indicators of coastal changes (Blasco et al. 1996) and have fluctuated throughout geological and human history. The area covered

by mangrove is influenced by complex interactions involving gradients of tidal flooding frequency, nutrient availability and soil salt concentration across the intertidal area (Hutchings and Saenger 1987; Wolanski et al. 1990). The geomorphological setting of mangrove systems also comprises a range of inter-related factors such as substrate types, coastal processes, sediment and freshwater delivery. All of these factors influence the occurrence and survival of mangroves (Semeniuk 1994).

Investigations along the littoral zone of the Brazilian Amazon using sedimentological, palynological and isotope data have revealed evidence of expansion/contraction of mangroves during the Holocene (Cohen et al. 2008, 2009; Lara and Cohen 2009; Guimarães et al. 2010, 2012; Smith et al. 2011, 2012). Those mangrove variations have been attributed to the combination of post-glacial sea-level rise (Suguio et al. 1985; Tomazelli 1990; Angulo and Suguio 1995; Martin et al. 1996; Angulo and Lessa 1997; Angulo et al. 1999; Rull et al. 1999; Hesp et al. 2007; Angulo et al. 2008), tectonic subsidence (Miranda et al. 2009; Castro et al. 2010; Rossetti et al. 2012) and changes in the discharge of the river Amazon as a consequence of variations in rainfall (Bush and Colinvaux 1988; Absy et al. 1991; Sifeddine et al. 1994; Desjardins et al. 1996; Gouveia et al. 1997; Pessenda et al. 1998a, 2001; Behling and Hooghiemstra 2000; Freitas et al. 2001; Sifeddine et al. 2001; Weng et al. 2002; Bush et al. 2007).

The mangroves of northern Brazil began to develop in their current position during the early and mid Holocene (Behling et al. 2001; Behling and Costa 2001; Cohen et al. 2005a; Vedel et al. 2006), due to the stabilization of relative sea-level (RSL) after the post-glacial sea-level rise that invaded the embayed coast and broad valleys (Cohen et al. 2005a; Souza Filho et al. 2006). Currently, the coastal zone influenced by the river Amazon (fluvial sector—northwestern coastline) is occupied by *várzea* freshwater herbaceous vegetation. However, pollen data indicate that marine influence and mangrove vegetation (brackish water vegetation) were more extensive than they are today on Marajó (Smith et al. 2011, 2012; França et al. 2012), as well as on the Macapá coast (Guimarães et al. 2012) between >8,800 and ~2,300 cal. B.P. and >5,500 and ~5,200 cal. B.P., respectively.

During the late Holocene, it is likely that the replacement of brackish or marine water by fresh water, which is indicated by vegetation at the mouth of the river Amazon, was caused by a wetter climate which generated an increase in river discharge (Bush and Colinvaux 1988; Absy et al. 1991; Desjardins et al. 1996; Pessenda et al. 1998a, 1998b; Freitas et al. 2001). A higher river discharge has maintained low tidal water salinity surrounding Marajó (0–6 ‰, Santos et al. 2008), while the marine-influenced littoral zone has a relatively higher tidal water salinity than

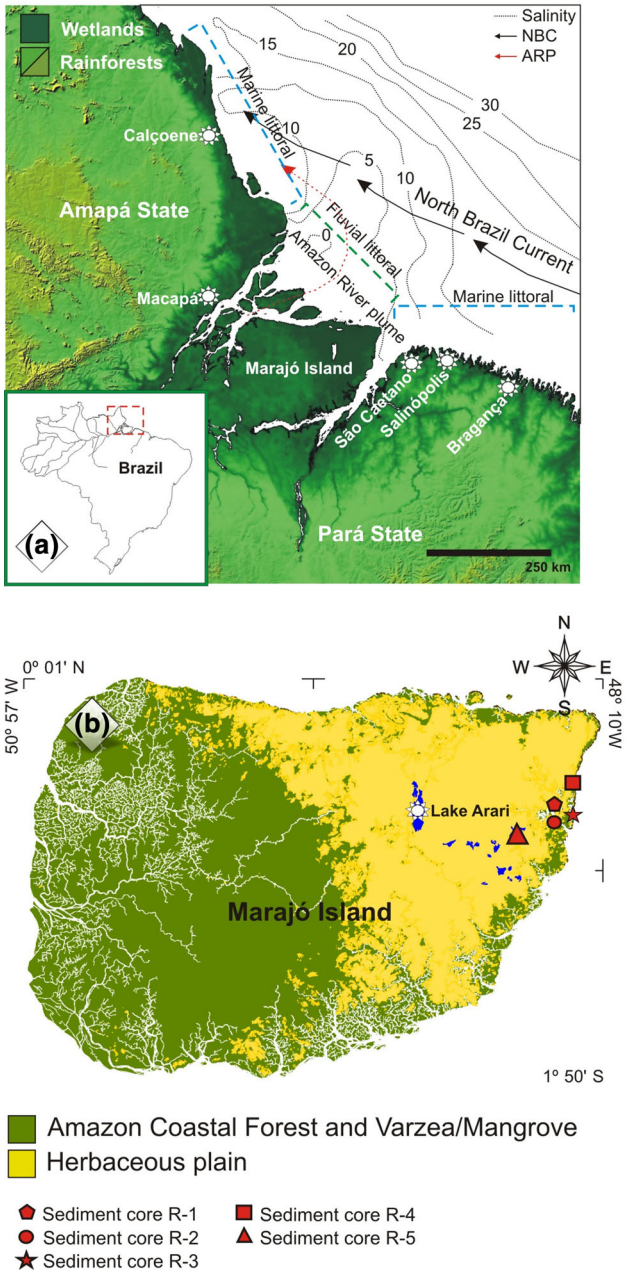

Fig. 1 Location of the study area **a** sea water salinity, river Amazon plume and North Brazil Current (Santos et al. 2008); **b** Ilha de Marajó, which covers approximately 40,000 km^2

the sector near the river Amazon (Fig. 1a, Cohen et al. 2012).

Previously, Smith et al. (2011) and França et al. (2012) indicated a contraction of mangroves on Marajó during the Holocene. The main objective of this investigation is to establish a relationship between the changes in estuarine salinity gradient from the river Amazon and the mangrove dynamics on the island of Marajó, northern Brazil. This study presents the integration of $\delta^{13}C$, $\delta^{15}N$, total organic carbon (TOC), C/N ratio, facies analysis and pollen data,

with a chronology from 15 radiocarbon samples. For this purpose, material extracted from five cores, with depths between 150 and 256 cm, was collected from the eastern coast of the island of Marajó.

Study site

Geological and geomorphological setting

The island of Marajó is situated in northern Brazil, on the coastal plain at the mouth of the river Amazon, and it has an area of about 40,000 km^2. The study sites are located in the central eastern region of this island (0°39′16.96″S/48°40′13.79″W to 0°55′51.35″S/48°28′16.96″W) (Cohen et al. 2008; Smith et al. 2011, 2012). Geologically, the island is located in the Pará Platform. The eastern margin has a topographical range of less than 5 m and extends inland to the maximum extent of the tidal influence zone, which limits the coastal plateau (França and Sousa Filho 2006). This region has a low relief, averaging only 4–6 m above modern sea-level (Rossetti et al. 2007, 2008, 2012), and is dominated by Holocene sedimentation, which is slightly depressed relative to the western side (Behling et al. 2004; Rossetti et al. 2007; Lara and Cohen 2009). Along the eastern portion, the Barreiras formation is represented by sandstones and mudstones followed by post-Barreiras deposits, that thicken toward the west in the subsurface (Rossetti et al. 2008).

Regional climate and oceanographic characteristics

The climate is warm and humid tropical, with an annual precipitation averaging 2,300 mm (Lima et al. 2005). The seasonality of regional precipitation is influenced by several factors, including the migration of the Inter Tropical Convergence Zone (ITCZ), due to changing Atlantic sea surface temperatures (SST), moist trade winds from the tropical Atlantic, evapotranspiration from the forest itself, and the coupled onset and intensity of Amazon convection (Marengo et al. 1993, 2001; Nobre and Shukla 1996; Fu et al. 2001; Liebmann and Marengo 2001). The rainy season occurs between the months of December and May, and a drier period between June and November. Average temperatures range between 25 and 29 °C. The region is dominated by a regime of semidiurnal meso- and macrotides with tidal ranges of 2–4 m and 4–6 m, respectively, with variations during the spring tide between 3.6 and 4.7 m (DHN 2003). The mean river Amazon discharge is about 170,000 m^3 s^{-1}, at the city of Óbidos, with maximum and minimum outflow of 270,000 and 60,000 m^3 s^{-1} (ANA 2003). Consequently, the river discharge and hydrodynamic conditions allow a strong reduction of water salinity along the Amazon and its adjacent coast (Fig. 1a; Vinzon et al. 2008; Rosario et al. 2009). Furthermore the structure of the river Amazon plume is controlled by the North Brazilian Current, which induces a northwestern flow with speeds of 40–80 cm s^{-1} over the continental shelf (Lentz 1995).

Modern vegetation

The modern vegetation consists of natural open areas dominated by herbaceous flats with Cyperaceae and Poaceae, which occur mainly on the eastern side of Marajó. The *várzea* vegetation, consisting of seasonal swamp and areas permanently inundated by freshwater, is composed of wetland trees such as *Euterpe oleraceae* and *Hevea guianensis,* while the vegetation on drier land, represented by the Amazon Coastal Forest (ACF) unit, is characterized by *Cedrela odorata*, *Hymenaea courbaril* and *Manilkara huberi* (Behling et al. 2004; Cohen et al. 2008; Smith et al. 2011, 2012). The *várzea* and ACF dominate the western side of Marajó (Fig. 1a). Narrow and elongated belts of dense ombrophilous forest are also present along riverbanks (Rossetti et al. 2008). The *restinga* shrub and herb vegetation that occurs on sand plains and on dunes close to the shore line is dominated by Anacardiaceae and Malpighiaceae. The mangroves are colonized by *Rhizophora*, *Avicennia* and *Laguncularia* (Cohen et al. 2008).

The mangrove on the studied island occurs within specific topographic zones (Cohen and Lara 2003; Cohen et al. 2005a, b, 2008, 2009), depending on physical characteristics such as sediment type (Duke et al. 1997) and chemical characteristics (Hutching and Saenger 1987; Wolanski et al. 1990), and is currently present in small areas on the northeastern coast, 100–700 m wide. The mangroves of our study area are classified as *Rhizophora*-dominated fringe forests reaching 20 m in height, with a presence of *Avicennia* at highest elevations above mean spring tide level, inundation frequency.

Materials and methods

Analysis of sedimentary facies, pollen, $\delta^{13}C$, $\delta^{15}N$, TOC and C/N ratio were conducted following the results of radiocarbon dating, to assess the development of the Amazonian mangrove and organic matter source. The sediment cores R-1, R-2 and R-3 were collected during the summer season in November 2008, using Russian type sampling equipment (Cohen 2003) and two others, R-4 and R-5, were sampled with a vibrocorer (Martin et al. 1995) using an aluminium tube.

Sampling

Five specific sites were selected for shallow coring, which represent different morphological aspects and vegetations on Marajó (Fig. 1b). The sediment cores were sampled from an area colonized by mangroves mainly characterized by *Rhizophora mangle* (R-4, S0°39′37″/W48°29′3″ and R-2, S0°40′23″/W48°29′38″) and mixed *várzea* and mangrove (R-1, S0°40′26″/W48°29′37″) characterized by *R. mangle* and other taxa such as Arecaceae (*E. oleracea, Mauritia flexuosa*), Araceae (*Montrichardia arborescens*), Aizoaceae (*Sesuvium*), Acanthaceae (*Avicennia germinans*), Cyperaceae, Heliconiaceae, Musaceae, Myrtaceae (*Psidium guajava*), Poaceae (*Olyra*) and Pteridaceae (*Acrostichum auereum*).

Core R-3 (S0°40′25″/W48°29′35″) was sampled from an area occupied by herbaceous and *restinga* vegetation characterized by Arecaceae (*E. oleracea*; *M. flexuosa*), Cyperaceae, Poaceae (*Olyra*), Malpighiaceae (*Byrsonima*), while core R-5 (S0°55′41″/W48°39′47″, 15 km from the shoreline) was sampled from an area colonized only by herbaceous vegetation mainly represented by Convolvulaceae, Rubiaceae, Cyperaceae and Poaceae.

Facies analysis

For analysis of sedimentary facies, the sediment cores were X-rayed to identify sedimentary structures and to aid in the analysis. The sediment grain size was obtained by laser diffraction using a SHIMADZU SALD 2101 laser particle size analyser in the Laboratory of Chemical Oceanography at UFPA. Approximately 0.5 g of each sample was rinsed with H_2O_2 to remove the organic matter, and residual sediments were disaggregated by ultrasound before the measurement of grain size (França 2010). The sediment grain size distribution follows the methods of Wentworth (1922), with distinction of the sand (2–0.0625 mm), silt (62.5–3.9 μm) and clay fractions (3.9–0.12 μm). The graphics were done using Sysgran (Camargo 1999), following the methods of Harper (1984) and Walker (1992). Facies analysis included description of colour (Munsell Color 2009), lithology, texture and structure. The sedimentary facies were codified following Miall (1978).

Pollen analysis

For pollen analysis, 1 cm^3 samples were taken at 2.5 cm intervals along sediment cores R-1, R-2 and R-3, giving a total of 183 samples, to develop a high resolution record of past vegetation changes. From sediment cores R-4 and R-5, 24 and 36 samples were collected, respectively. Prior to processing, one tablet of exotic *Lycopodium* spores (Stockmarr 1971) was added to each sediment sample to allow the calculation of pollen concentration (grains cm^{-3}) and pollen accumulation rates (grains cm^{-2} $year^{-1}$). All samples were prepared using standard analytical techniques for pollen including acetolysis (Fægri and Iversen 1989). Sample residues were placed in Eppendorf microtubes and kept in a glycerol gelatin medium. Reference morphological descriptions (Roubik and Moreno 1991; Behling 1993; Herrera and Urrego 1996; Colinvaux et al. 1999) and the reference pollen collection of the Laboratory of Coastal Dynamics at the Federal University of Pará were consulted for identification of pollen grains and spores. A minimum of 300 pollen grains were counted in each sample. The pollen sum excludes fern spores, algae and micro-foraminifers. Pollen and spore data are presented in diagrams as percentages of the pollen sum (França et al. 2012). Taxa are grouped into mangrove, herbaceous plain elements, *Restinga* (coastal forest vegetation), palms, and ACF. Tilia and Tilia.Graph were used to calculate and plot the pollen diagrams (Grimm 1987).

Organic geochemistry

A total of 236 samples (6–50 mg) were collected at 5 cm intervals from the sediment cores in order to associate the vegetation changes and also to understand the changes in organic matter source. Samples of leaves, roots, etc., were separated and treated with 4 % HCl to eliminate carbonates, washed with distilled water until the pH reached 6, dried at 50 °C and homogenized. These samples were used for TOC and nitrogen analyses, carried out at the Stable Isotope Laboratory of the Center for Nuclear Energy in Agriculture (CENA/USP). The results are expressed as a percentage of dry weight, with analytical precision of 0.09 and 0.07 %, respectively. The ^{13}C and ^{15}N results are expressed as $\delta^{13}C$ and $\delta^{15}N$ with respect to the VPDB standard and atmospheric air, respectively, using the following conventional notations:

$$\delta^{13}C\ (‰) = [(R_{1sample}/R_{2standard}) - 1] \cdot 1{,}000$$
$$\delta^{15}N\ (‰) = [(R_{3sample}/R_{4standard}) - 1] \cdot 1{,}000$$

where $R_{1sample}$ and $R_{2standard}$ are the $^{13}C/^{12}C$ ratio of the sample and standard, as well as $R_{3sample}$ and $R_{4standard}$ are the $^{15}N/^{14}N$, respectively. Analytical precision is ± 0.2 ‰ (Pessenda et al. 2004).

Surface sample sediment cores were collected to verify the isotopic composition of modern organic matter, and to compare the different isotopic signatures among them. Leaves of the most representative trees of the study area were also sampled for $\delta^{13}C$ determination, to define photosynthetic characteristics of regional vegetation (ESM 1). The application of carbon isotopes is based on the ^{13}C composition of C_3 (trees) and C_4 (grasses) plants and their preservation in SOM (sedimentary organic matter). Especially in the Amazon ecosystem with a predominance of C_3 plants, the isotope values tend to increase towards the deeper layers,

around 3–4 %, caused by the fractionation during decomposition of organic matter. However, if the ^{13}C enrichment with depth is large, it is a stronger indication that the signal is due to the previous existence of ^{13}C-enriched vegetation, probably C_4 grasses. (Martinelli et al. 1996, 2003).

The $\delta^{13}C$ values of C_3 plants range from approximately −32 to −20 ‰ VPDB, with a mean of −27 ‰. In contrast, $\delta^{13}C$ values of C_4 species range from −17 to −9 ‰, with a mean of −13 ‰.

The organic matter source is environment-dependent with different $\delta^{13}C$, $\delta^{15}N$ and C/N compositions (Lamb et al. 2006) as follows: the C_3 terrestrial plants show $\delta^{13}C$ values between −32 and −20 ‰ and C/N ratio >20, while C_4 plants have $\delta^{13}C$ values ranging from −17 to −9 ‰ and C/N >35 (Deines 1980; Meyers 1994; Tyson 1995; Lamb et al. 2006). In C_3-dominated environments, freshwater algae have $\delta^{13}C$ values between −25 and −30 ‰ (Meyers 1994; Schidlowski et al. 1983) and marine algae between −24 and −16 ‰ (Haines 1976; Meyers 1994). In C_4-dominated environments, algae can have $\delta^{13}C$ values ≤16 ‰ (Chivas et al. 2001). Bacteria have $\delta^{13}C$ values ranging from −12 to −27 ‰ (Coffin et al. 1989). In general, bacteria and algae have C/N values of 4–6 and <10, respectively (Meyers 1994; Tyson 1995).

Fluvial $\delta^{13}C_{POC}$ values (POC; particulate organic carbon) result from freshwater phytoplankton and estuarine dissolved organic carbon (DOC) (−25 to −30 ‰) and particulate terrestrial organic matter (−25 to −33 ‰). However, marine $\delta^{13}C_{POC}$ ranges from −23 to −18 ‰ (Barth et al. 1998; Middelburg and Nieuwenhuize 1998). Peterson et al. (1994) found values from marine $\delta^{13}C_{DOC}$ between −22 and −25 ‰ and freshwater values between −26 and −32 ‰. Thornton and McManus (1994) and Meyers (1997) used $\delta^{15}N$ values to differentiate organic matter from aquatic (>10 ‰) and terrestrial plants (∼0 ‰).

The plants of aquatic environments normally use dissolved inorganic nitrogen, which is isotopically enriched in ^{15}N by 7–10 ‰ relative to atmospheric N_2 (0 ‰), thus terrestrial plants that use N_2 derived from the atmosphere have $\delta^{15}N$ values ranging from 0 to 2 ‰ (Thornton and McManus 1994; Meyers 2003).

The geochemical analyses also included a binary diagram between $\delta^{13}C$ and C/N for each sedimentary core in the study area in order to show information such as the origin of organic matter preserved in this region (Haines 1976; Deines 1980; Schidlowski et al. 1983; Meyers 1994; Peterson et al. 1994; Tyson 1995; Middelburg and Nieuwenhuize 1998; Raymond and Bauer 2001; Lamb et al. 2006).

Radiocarbon dating

The chronological framework for the sedimentary sequence was provided by conventional and accelerator mass spectrometer radiocarbon dating. 15 bulk samples of 10 g each were selected, according to stratigraphic discontinuities that suggested past changes in the tidal inundation regime. In order to avoid natural contamination (Goh 2006), the sedimentary samples were checked and physically cleaned under a stereomicroscope. The organic matter was chemically treated to remove any more recent organic material such as fulvic and/or humic acids, and carbonates. This process consisted of extracting residual material with 2 % HCl at 60 °C for 4 h, washing with distilled water to neutralize the pH, and drying at 50 °C. A detailed description of the chemical treatment for sediment samples can be found in Pessenda and Carmargo (1991) and Pessenda et al. (1996). The samples were analyzed at the radiocarbon laboratory of CENA/USP and at UGAMS (University of Georgia–Center for Applied Isotope Studies). Radiocarbon ages were normalized to a $\delta^{13}C$ of −25 ‰ VPDB and reported in the stratigraphical columns as calibrated years (cal. year B.P., 2σ range) using Calib 6.0 (Stuiver et al. 1998; Reimer et al. 2004, 2009). The dates are given in the text as the median of the range of calibrated ages in our data and that of other authors (ESM 2), with some ages estimated by linear extrapolation based on sedimentation rate. The sedimentation rates were based on the ratio between the depth intervals in mm and the time range.

Results

Radiocarbon dates and sedimentation rates

Radiocarbon dates for cores R-1 to R-5 (Franca et al. 2012) are shown in ESM 2. Sedimentation rates are between 0.1 and 10 mm $year^{-1}$. Although the rates are non-linear between the dated points, they are within the vertical accretion range of 0.1–10 mm $year^{-1}$ of mangrove forests as reported by other authors (Bird 1980; Spenceley 1982; Cahoon and Lynch 1997; Behling et al. 2004; Cohen et al. 2005a, 2008, 2009; Vedel et al. 2006; Guimarães et al. 2010).

$\delta^{13}C$ values of modern vegetation

22 taxa of the most representative vegetation were collected at the study site. Their $\delta^{13}C$ values range between −34.23 and −27.23 ‰, and indicate a predominance of C_3 plants (ESM 1). The contribution of C_4 to the $\delta^{13}C$ signal in the sediment is restricted to the Poaceae (unidentified) with a mean value of −12.24 ‰, and Aizoaceae (*Sesuvium*) with a value of −13.94 ‰.

Facies, pollen description and isotope values of the sediment cores

The cores consisted of dark grey and light brown muddy and sandy silt sediments with an increase in grain size towards

Table 1 Summary of facies association, pollen, isotopes and C/N values, with the proposed interpretation of the depositional environments

Facies assoc.	Facies description	Pollen, isotopic and C/N values	Interpretation
A	Plastic, massive mud with many roots and root marks (facies Mm), with dwelling structures (facies Mb). Fine grained sand (facies Mms) to very fine grained sand (facies Mp), pale olive silty sand with light grey mottles, many roots and roots traces in growth position and dwelling structures (facies Sb), lenticular heterolithic (facies Hl) and fine to medium-grained cross-stratified sand (facies Sc), with continuous streaks of grey to olive	Pollen = mangrove vegetation $\delta^{13}C = -29.3$ to -26.9 ‰ $\delta^{15}N = -0.6$ to 5.0 ‰ C/N = 11.9 to 45.6	Mangrove tidal flat
B	Plastic, massive mud, grey to dark grey and green, with many roots and root marks (facies Mm), with traces in growth position and dwelling structures (facies Sb). These deposits also have sandy-silt sediments	Pollen = mangrove and herbs vegetation $\delta^{13}C = -27.8$ to -26.4 ‰ $\delta^{15}N = 0.0$ to 3.9 ‰ C/N = 11.1 to 36.3	Mangrove/ herbaceous flat
C	Light yellow, moderately sorted, fine-grained massive sand. Mud intraclasts are either dispersed or locally form conglomeratic lags (facies Sm) and massive mud with many roots and root marks (facies Mm), preceding the facies association C	Pollen = mangrove vegetation, ACF and herbs vegetation $\delta^{13}C = -25.8$ to -27.6 ‰ $\delta^{15}N = 2.2$ to 2.4 ‰ C/N = 23.8 to 24.2	Lagoon
D	Fine to medium grained sand with parallel lamination or stratification (facies Sp). Local association with mud drape and mud intraclasts are either dispersed or locally form conglomeratic lags (facies Sm). Grey mud layers interbedded with fine to medium grained sand forming *flaser* structures (facies Hf) and *wavy* structures (facies Hw)	Pollen = no pollen $\delta^{13}C = -27.6$ to -25.0 ‰ $\delta^{15}N = 2.2$ to 2.6 ‰ C/N = 22.2 to 24.2	Foreshore
E	Massive mud with many roots and root marks (facies Mm) and dwelling structures and diffuse fine sand following the root traces and benthic tubes (facies Mb)	Pollen = ACF, herbs and aquatic vegetation $\delta^{13}C = -22.7$ to -25.5 ‰ $\delta^{15}N = 1.7$ to 6.0 ‰ C/N = 18.7 to 24.2	Lake

the top. These deposits are massive, parallel laminated or heterolithic. The texture analysis and sediment descriptions of the materials collected in the tidal flat, together with pollen records, isotopic ($\delta^{13}C$ and $\delta^{15}N$), TOC and C/N values, have allowed five facies associations to be defined (Table 1).

R-1 core (mangrove/várzea, 150 cm)

This core is marked by facies associations B and A (Table 1). These deposits consist mainly of massive (macroscopically homogenous sedimentary deposit without any features) mud with many roots and root marks with dwelling structures caused by the activity of organisms in the sediment (facies Mm and Mb). There is clay, silt and fine sand with flat lenses of rippled sand (facies HI). The top layer displays fine to medium-grained sand (facies Sb). The R-1 core is of mud with convolute laminations (Fig. 2, 90–80 cm), produced by localized differential forces acting on a hydroplastic sediment layer, a formation which is commonly found on mud flats (Collinson et al. 2006).

The pollen and spore analysis results have been divided into five ecological groups (Fig. 2), which are also present in the other profiles. Zone R1#1 (150–135 cm) is characterized by a predominance of herbaceous pollen and also by pollen taxa of *restinga*, ACF and the palms group. The mangrove pollen declines slightly. Zone R1#2 (135–0 cm) is marked by a significant increase of mangrove pollen, followed by a decrease of herbaceous pollen, and that from ACF, *Restinga* and the palms group.

The organic geochemistry results are presented in Fig. 2, and indicate that $\delta^{13}C$ values are greater in the bottom layer (mean -27 ‰) than in the surface layer (around -29 ‰). The $\delta^{15}N$ values range from 0.0 to $+3.3$ ‰ toward the surface, and C/N values are between 36 and 13, with high values at the bottom and low values toward the surface. The TOC results show a decreasing trend from bottom to surface, with values between 14 and 1 %, respectively.

R-2 core (mangrove, 150 cm)

These deposits consist typically of massive mud (facies Mm), bioturbated mud (facies Mb) and coarse to fine-grained sand (facies Sb), with an increase in sandy

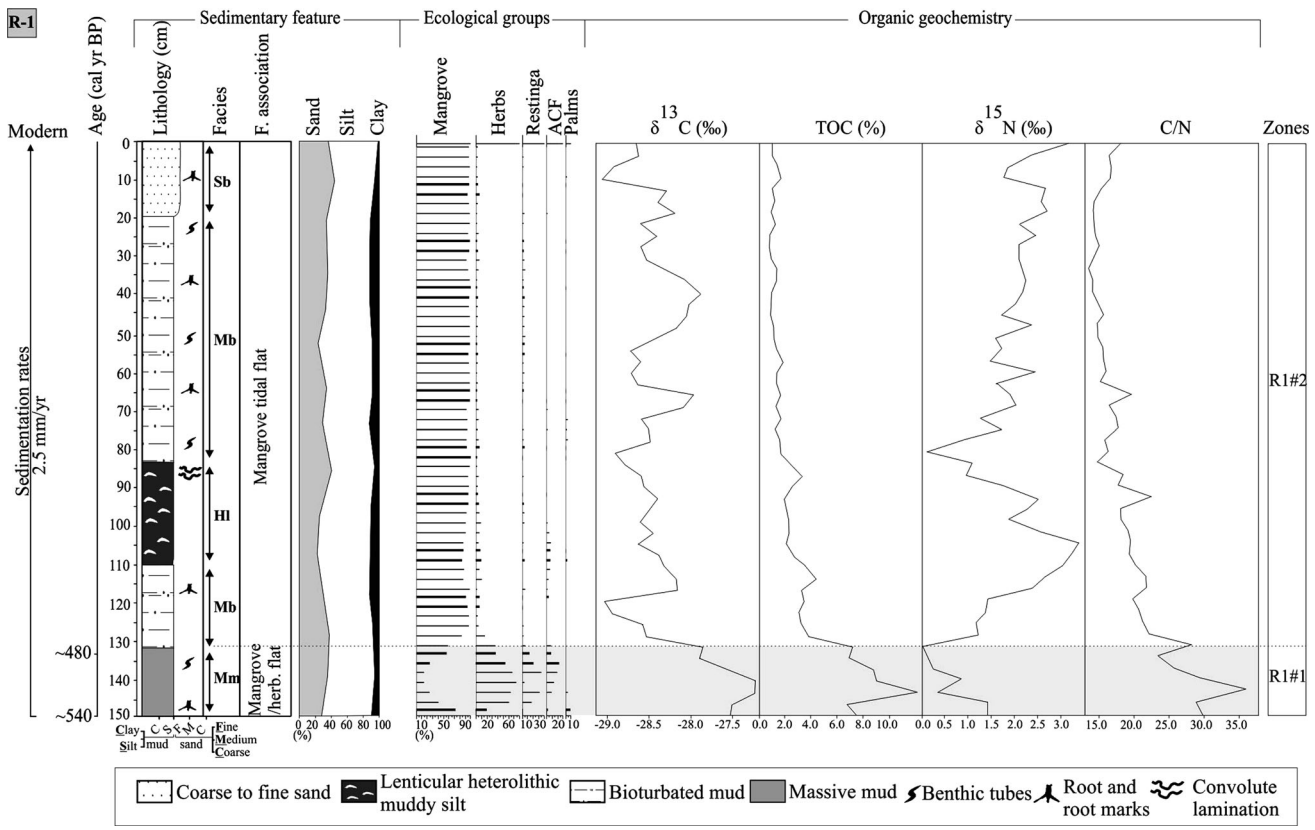

Fig. 2 Summary results for R-1 core: variation as a function of core depth from chronological, lithological profile, pollen analysis and geochemical variables

sediments at the surface layers. They also have many roots and root holes with animal burrows (Fig. 3). The core typically shows two facies associations B and A, representing mangrove/herbaceous flat and mangrove tidal flat, respectively (Table 1).

The results of the pollen and spore analyses are given in five ecological groups (Fig. 3). The interval between 150 and 95 cm is characterized by herbaceous and mangrove pollen, while the top sequence is dominated by mangrove.

The organic geochemistry results provide isotope and elemental data that indicates $\delta^{13}C$ values decreasing in the upper part of the core, from −26 to −29 ‰, while the $\delta^{15}N$ values oscillate between −0.6 and +3.9 ‰. The C/N also decreases in the upper part of the core, from 35 to 16. The TOC values range between 0.5 and 7.9 %. (Fig. 3).

R-3 core (herbaceous plain/mangrove, 150 cm)

The core consists of bioturbated muds (facies Mb), which are interbedded with lenticular muddy silts (facies Hl) and cross-lamination of sand (facies Sc). Near the top there is fine to medium-grained sand (facies Sb), with an increase in grain size towards the top. This core has facies associations A and B (Table 1), with mangrove tidal flat and mangrove/herbaceous flat (Fig. 4).

The interval between 150 and 15 cm shows a dominance of mangrove pollen, while the top has a decrease in mangrove, and an increase in herbaceous pollen and trees and shrubs from ACF.

The isotope data and elemental analysis results are presented in Fig. 4. The $\delta^{13}C$ values oscillate between −28.3 and −27 ‰. The $\delta^{15}N$ values increase from bottom to top, from +0.6 to +4.8 ‰. The C/N decreases from 26.2 at the base to 11.1 at the surface. The TOC values are between 0.3 and 2 %, with higher values at 120 cm.

R-4 core (mangrove, 225 cm)

These deposits are mainly sandy sediments at the bottom, with mud present higher up the profile. This core grades downward into heterolithic deposits (facies Hf and Hw), consisting of massive sand (facies Sm) or, less commonly, parallel laminated, fine to very fine-grained sand (facies Sp). Plant debris and overload structures are locally present. These deposits have associations D, C and A (Table 1), representing a phase of foreshore, with tidal channel (facies Hf and Hw), lagoon with mangrove and mangrove tidal flat, respectively (Fig. 5).

The interval 225–70 cm is characterized by an absence of pollen, probably due to the presence of sandy sediments,

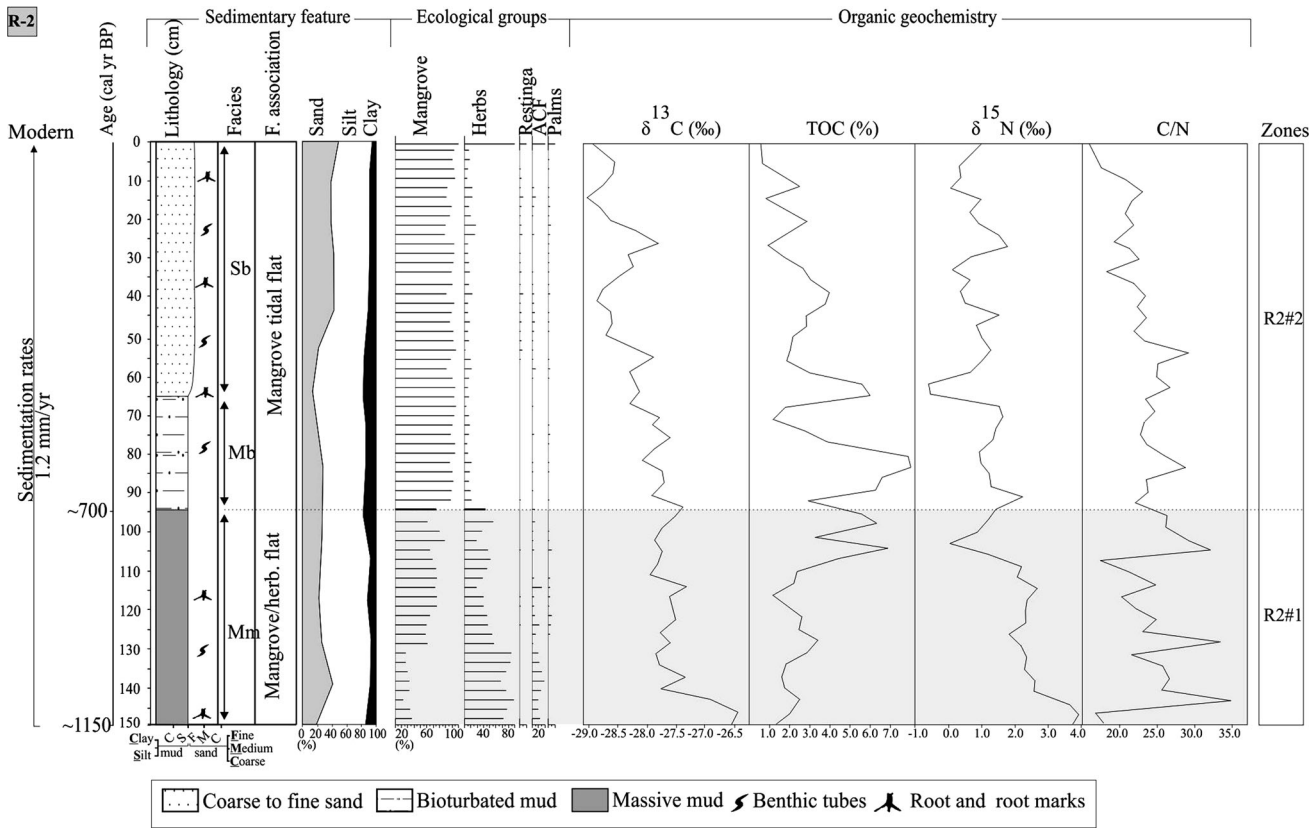

Fig. 3 Summary results for R-2 core: variation as a function of core depth from chronological, lithological profile, pollen analysis and geochemical variables

coinciding with a foreshore facies association, while the section between 70 and 40 cm is marked by the onset of mangrove development. The top (40–0 cm) is marked by an increase of mangrove pollen, characterizing the mangrove tidal flat facies association.

The organic geochemical results obtained in the bottom zone had $\delta^{13}C$ values between −27 and −25 ‰ and TOC values around 0–1 %. Higher up in the profile, where mangrove occurs, the $\delta^{13}C$ values were lower (between −26 and −29 ‰). Modern sediments show $\delta^{15}N$ results between +0.5 and +2.5 ‰ and C/N decreasing to approximately 18 at the surface. The TOC values were 0 % between 225 and 80 cm, increasing higher up in the profile to 9 % at the top (Fig. 5).

R-5 core (lake/herbaceous plain, 256 cm)

The sediment consisted typically of massive mud (facies Mm) and parallel laminated mud (facies Mp), with plant fragments, leaves and benthic structures. Near the surface there was bioturbated mud (facies Mb). These deposits have characteristics related to associations A and E (Fig. 6; Table 1), indicating a phase of a mangrove tidal flat and a lake stage, respectively.

The base of this core is marked mainly by mangrove pollen (255–55 cm), while the top shows a decrease of mangrove pollen, which is replaced by herbaceous and ACF pollen (55–0 cm).

The organic geochemical results show a contrast between the two depositional periods (Fig. 6). During the time interval ~7,500 B.P. to ~3,200 cal. B.P. (estimated age), the mangrove tidal flat was characterized by $\delta^{13}C$ values between −28 and −25 ‰. The $\delta^{15}N$ results during the mangrove phase were +1 to +5 ‰ and C/N values between 9 and 45. The TOC results from the bottom of the core were relatively higher (2.6–4.9 %) than in the middle (0.9–2.7 %), and at the top around 6 %. The upper facies, deposited by the lake since ~3,200 cal. B.P., shows $\delta^{13}C$ values increasing from −26.5 to −22 ‰. The $\delta^{15}N$ values were between 1 and 6 ‰, C/N values around 17 and 20 and there was an increase in the TOC concentration to 6 %.

Interpretation and discussion

Generally, sediment cores sampled from lakes include pollen and organic matter sourced from the lake and its surroundings (Davis 2000; Xu et al. 2012), while cores sampled from tidal flats receive pollen and organic matter

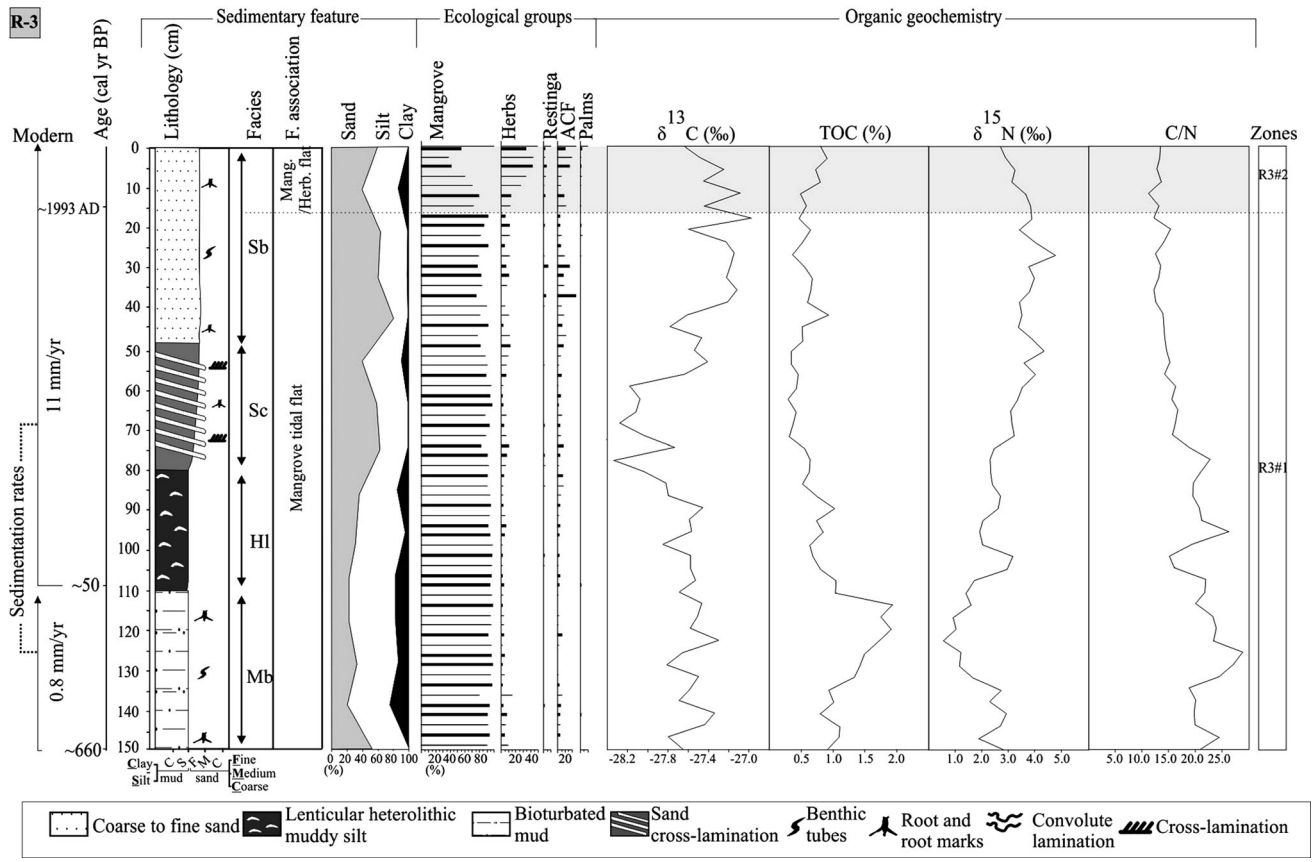

Fig. 4 Summary results for R-3 core: variation as a function of core depth from chronological, lithological profile, pollen analysis and geochemical variables

from relatively near to the sampling site (Behling et al. 2001). For this reason, core R-5, which was sampled from a lake in the central region of the island between depths of 0 and 55 cm, is probably more representative of the more regional vegetation and organic matter of eastern Marajó than the records from cores R-1, R-2, R-3 and R-4, which were collected from tidal flats with smaller catchment areas for vegetation and organic matter (Cohen et al. 2008; Smith et al. 2011, 2012).

Thus, the results obtained from sedimentary features, pollen and geochemical analyses from Marajó suggest significant changes in vegetation and organic matter sources during at least the last 7000 years. The data suggest that there were three phases, the first a tidal flat colonized by mangrove in the central region of the island between ~7,500 and ~3,200 cal. B.P. (estimated age), and with relatively higher contributions of estuarine organic matter between ~7,500 and ~6,500 cal. B.P., as recorded in core R-5 (Figs. 6, 7, 8). From ~3,200 to ~1,150 cal. B.P. in the hinterland of Marajó, the mangroves were largely replaced by herbaceous vegetation, characterizing the second phase. The third phase is marked by migration and isolation of mangrove to the east coast of the island from ~1,150 cal. B.P. at the earliest, as shown in core R-2, and this is also shown in cores R-1, R-4 and R-3 at ~540, ~580 and ~660 cal. B.P., respectively (Fig. 8).

First phase; mangrove (early to mid-Holocene, ~7,500 to ~3,200 cal. B.P.)

The tidal mud flats were occupied by mangroves from at least ~7,500 cal. B.P., and remained in the area of R-5 until ~3,200 cal. B.P. (Fig. 8). The relationship between $\delta^{13}C$ and C/N values indicates the influence of estuarine organic matter, with dominance of C_3 plants with $\delta^{13}C$ values −32 to −21 ‰ (Deines 1980) and a mixture of freshwater algae with $\delta^{13}C$ values of −26 to −30 ‰ (Schidlowski et al. 1983; Meyers 1994), and with brackish water algae shown by $\delta^{13}C$ values −22 to −25 ‰ (Peterson et al. 1994). The $\delta^{13}C$ values around −27 ‰ of organic matter recorded during this phase are 3 ‰ enriched in relation to the $\delta^{13}C$ values range of mangrove vegetation at −33 to −30 ‰ (ESM 1). Pollen percentages are between 60 and 95 %, with some herbs including some C_3 ones. These differences in isotope values may be attributed to the natural trend of $\delta^{13}C$ to increase in the deeper layers from

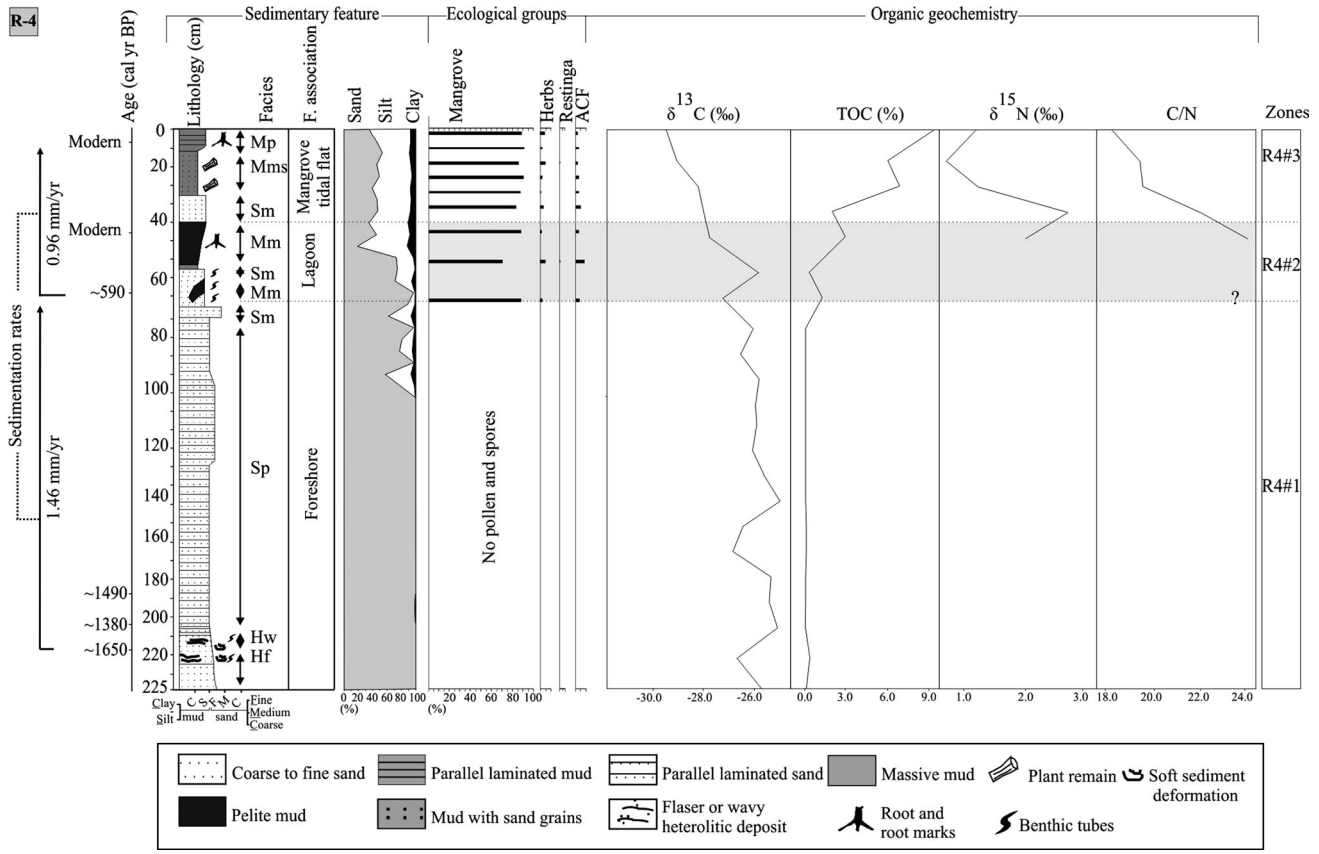

Fig. 5 Summary results for R-4 core: variation as a function of core depth from chronological, lithological profile, pollen analysis and geochemical variables

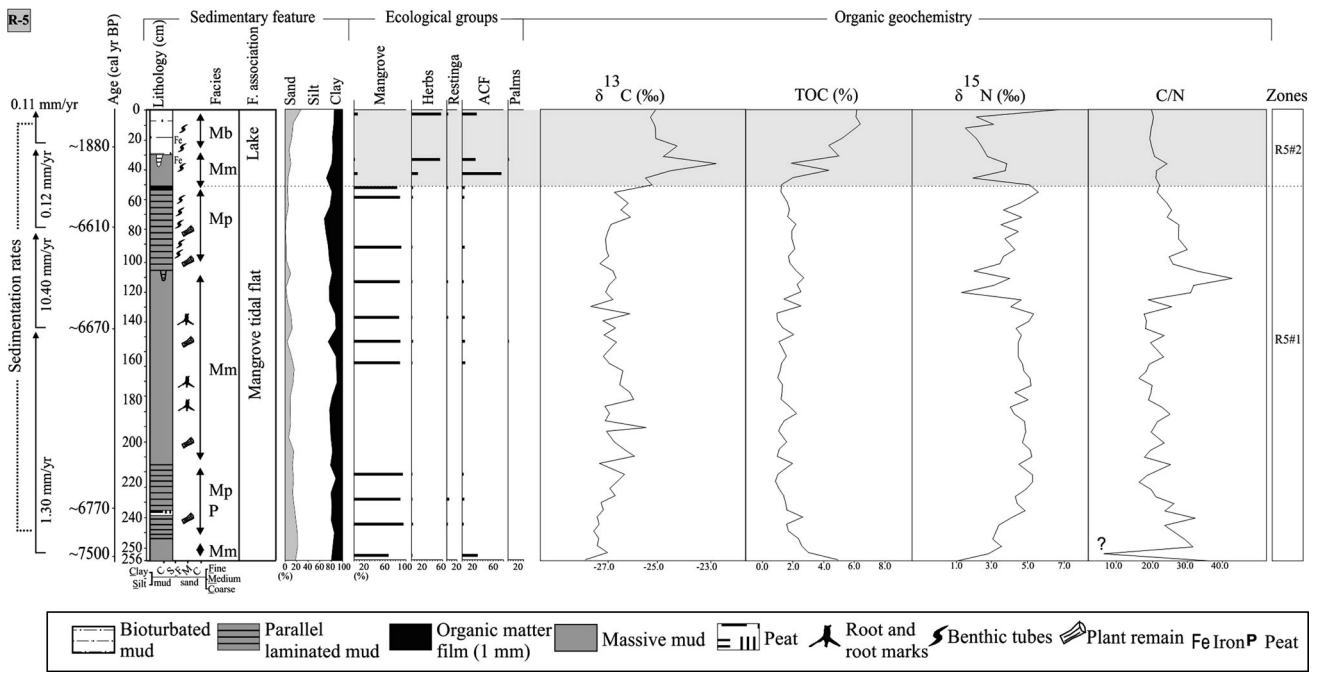

Fig. 6 Summary results for R-5 core: variation as a function of core depth from chronological, lithological profile, pollen analysis and geochemical variables

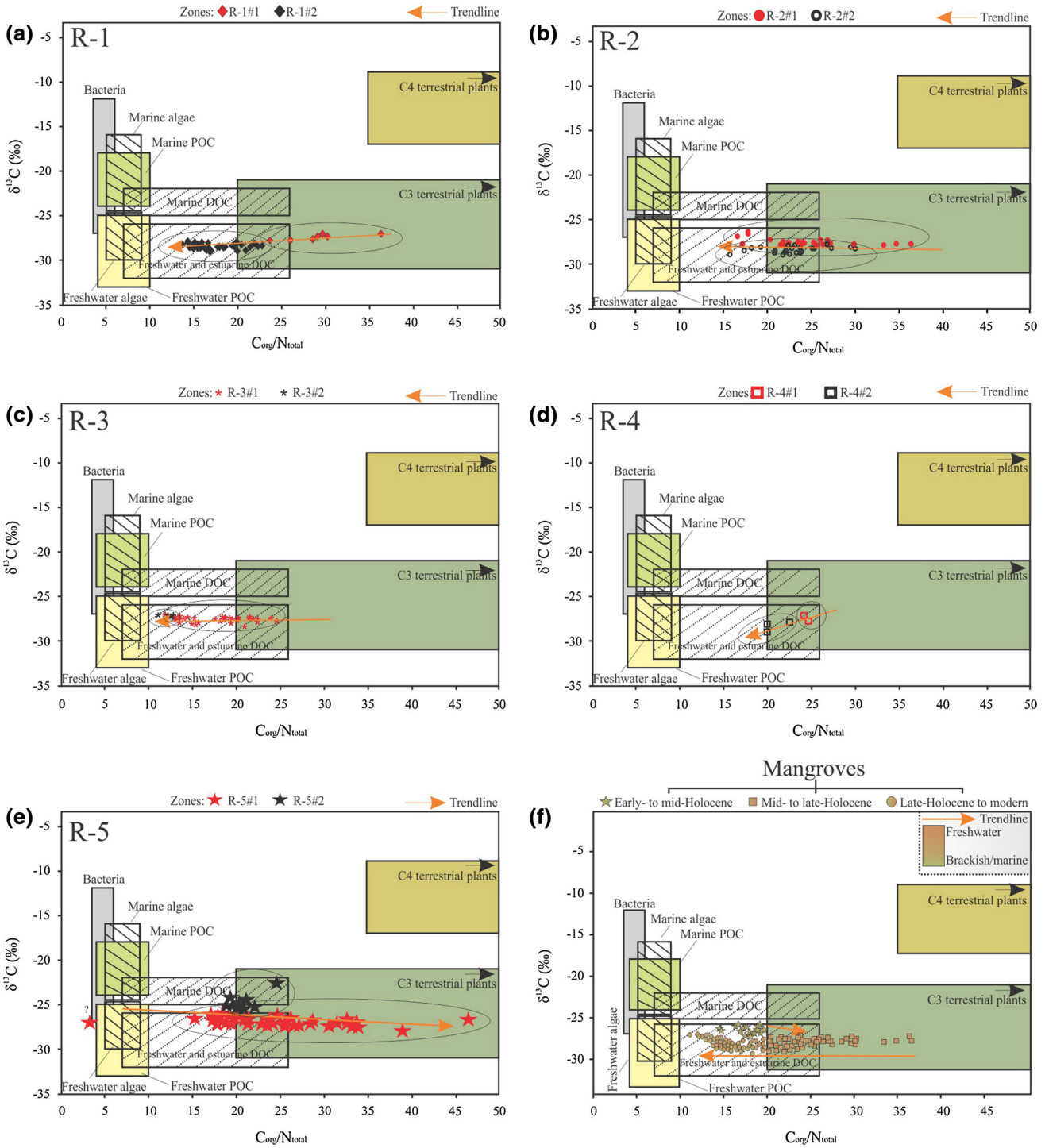

Fig. 7 Binary diagram between $\delta^{13}C$ x C/N for the different studies cores and different zones: **a** R-1; **b** R-2; **c** R-3; **d** R-4 and **e** R-5 core. 7f represents the integration of $\delta^{13}C$ and C/N data of organic matter preserved along the facies association mangrove tidal flat. The different fields in the $\delta^{13}C \times$ C/N plots correspond to the member sources for organic matter preserved in sediments and trend line, on red line (modified from Meyers 1997 and Lamb et al. 2006)

around 3–4 ‰, which is caused by the fractionation during decomposition of organic matter. The $\delta^{15}N$ values of 1.3–5 ‰ suggest a mixture of terrestrial plants and aquatic organic matter ($\sim$5 ‰, Sukigara and Saino, 2005). The C/N values at 15–42 also indicate a mixture of organic matter from vascular plants and algae, since values <10 show that algae dominate and >12 show vascular plants being dominant (Meyers 1994; Tyson 1995).

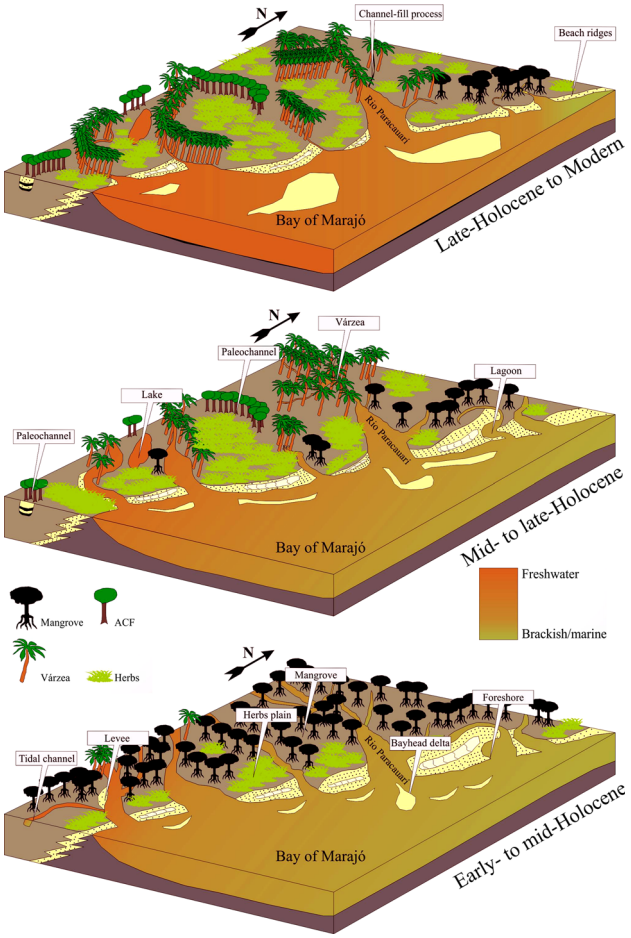

Fig. 8 Schematic representation of successive phases of sediment accumulation and vegetation change in the study area according to marine-freshwater influence gradient

Second phase; lake (mid to late Holocene, ~3,200 to ~1,880 cal. B.P.)

This phase is marked by massive mud sedimentation, with a 1 mm thick film of organic matter and some benthic tubes, root and root holes (R-5, 42 cm) that indicate stagnant conditions with vegetation development indicating herbaceous plain and ACF influences. The relationship between $\delta^{13}C$ values of −25.5 to −22.7 ‰ and C/N values <20 indicate a mixture of continental organic matter, dominance of C_3 plants with a slight component of C_4 herbaceous plant influence, and some aquatic contribution (Figs. 6,7d, 8), suggesting that there was a lake there since ~3,200 cal. B.P. at the earliest. During this stage there is a reduction of mangrove (<8 %) and its replacement by herbaceous vegetation (20–55 %), ACF (30–75 %) and some aquatic elements with freshwater influence. The interruption of mangrove development during this period indicates unfavourable conditions for mangroves, which may have been due to a decrease in salinity of the water in sediment pores (porewater). During this interval, the ACF and herbaceous plain taxa, which had adapted to freshwater flooding, expanded in this area. The mangroves were isolated in the most northeastern areas of Marajó, about 40 km away from the site of the R-5 core, where the tidal water salinity remained relatively higher.

Third phase; mangrove (late Holocene to modern, since ~1,700 cal. B.P.)

The foreshore facies association (R-4, Fig. 5) was recorded between ~1,700 and ~600 cal. B.P. This period is marked by low TOC and absence of pollen. It may be caused by various external factors such as sediment grain size, microbial attack, oxidation and mechanical forces, as well as factors inherent to the pollen grains themselves, such as sporopollenin content, chemical and physical composition of the pollen wall (Havinga 1967). In this case, the sediment grain size and energy flow can be considered the main causes of the absence of pollen, since the sandy sediments are not favourable to pollen preservation.

It was not possible to measure the C/N and $\delta^{15}N$ values of the foreshore facies association, due to low concentration of nitrogen in sedimentary organic matter. Thus, it is not possible to identify the origin of the organic matter preserved in these sediments as either terrestrial or marine. The $\delta^{13}C$ values around −26 ‰ may indicate continental C_3 plants (−32 to −21 ‰, Deines 1980) and/or freshwater algae (−26 to −30 ‰, Schidlowski et al. 1983; Meyers 1994).

This phase is marked by the presence of mangrove from ~1,150 cal. B.P. (R-2) at the earliest, and is recorded in cores R-1, R-4 and R-3 at ~540, ~580 and ~660 cal. B.P., respectively. Data presented by Behling et al. (2004) shows that mangrove vegetation became established at about ~2,800 cal. B.P. along the northeastern coast of Marajó. The vegetation development in this region was marked by four ecological groups, herbs, *Restinga*, ACF and palms.

During the last thousand years the relationship between $\delta^{13}C$ and C/N shows a trend from continental organic matter to that originating from estuarine algae during mangrove establishment (Fig. 7). This indicates an increase in tidal influence on the R-1, R-2, R-3 and R-4 areas, mainly during the last century.

River Amazon and relative sea level (RSL) controlling mangrove dynamics

Climate change within the Holocene there is often suggested as the cause of the modern biodiversity and biogeography of Amazonia (Bush 1994; Colinvaux 1998; Bush et al. 2004; Weng et al. 2004; Hermanowski et al. 2012). The main climatic factors which may have driven changes in vegetation are temperature, precipitation, seasonality and CO_2 concentration (Bush et al. 2004). However, the development

of mangroves is regulated by continent-ocean interactions and their expansion is determined by the topography relative to sea-level (Gornitz 1991; Cohen and Lara 2003), and flow energy (Woodroffe 1989; Chapman 1976), where mangroves preferentially occupy mud surfaces. On the tidal mud flats, this ecosystem is controlled by tidal inundation frequency, nutrient availability and water salinity (Hutchings and Saenger 1987; Lara and Cohen 2006). Mangroves are tolerant of soil salinity, which is mostly controlled by flooding frequency (Cohen and Lara 2003) and estuarine salinity gradients (Lara and Cohen 2006).

Therefore, despite the fact that mangroves are influenced by coastal variables (Blasco et al. 1996), climatic changes recorded in the Amazon basin during the Holocene (Absy et al. 1991; Desjardins et al. 1996; Gouveia et al. 1997; Pessenda et al. 1998a) must have affected the discharge of the river Amazon, and consequently, its estuarine salinity gradients and the area flooded by estuarine waters at the river mouth (Smith et al. 2011; 2012; Guimarães et al. 2012).

The data indicate a tidal mud flat colonized by mangroves with influence of estuarine organic matter between at least ~7,500 and ~3,200 cal. B.P. (Figs. 7f, 8). This was probably due to the relatively greater marine influence caused by reduced discharge of the Amazon, itself a result of a dry period during the early and middle Holocene (Pessenda et al. 2001; Behling and Hooghiemstra 2000; Freitas et al. 2001; Sifeddine et al. 2001; Weng et al. 2002; Bush et al. 2007). Mangrove expansion during the early Holocene was probably caused by the post-glacial sea-level rise which, combined with tectonic subsidence (Rossetti et al. 2008, 2012), led to a marine transgression. This event caused a marine incursion along the littoral of northern Brazil, where the RSL stabilized at its current level between 7000 and 5000 year B.P. (Cohen et al. 2005a; Vedel et al. 2006). A transgressive phase occurred on Marajó in the early to middle Holocene. Subsequently, there was a return to more continental conditions like those in the study area now (Rossetti et al. 2008).

During the late Holocene, there was a decrease of mangroves in the area of R-5 and the contribution of freshwater organic matter is higher than in the early and middle Holocene (Fig. 7f), suggesting a decrease in marine influence as recorded by Smith et al. (2012). This led to the isolation of mangroves in the eastern part of Marajó since at least ~1,150 cal. B.P. (Fig. 3), indicating a gradual migration of mangroves from the central region to the current coastline (Fig. 8). An increase in Amazon discharge during the wetter late Holocene in the northern and northeastern regions of Brazil (Pessenda et al. 1998a, 2001, 2004, 2010) may have resulted in this isolation (Guimarães et al. 2012; Smith et al. 2011, 2012). This process could be responsible for the modern decrease in tidal water salinity along the littoral (0–6 ‰, Santos et al. 2008). It is clearly observed in the relationship between C/N and $\delta^{13}C$ (Fig. 7), which shows a trend of increasing aquatic organic matter (R-1, R-2, R-3 and R-4).

Conclusions

The sediment deposits from Marajó offer a valuable opportunity to investigate past climate and RSL, and their effects on vegetation and sedimentary organic matter. Changes in vegetation, sediment deposition and organic matter input should be related to the interaction between the Amazon climate and the RSL. The data indicate a tidal mud flat colonized by mangroves with estuarine organic matter in the interior of Marajó between ~7,500 and ~3,200 cal. B.P., caused by the post-glacial sea-level rise, which combined with tectonic subsidence, produced a marine transgression. The relatively greater marine influence in the studied area was probably favoured by reduced Amazon discharge, in turn caused by a dry period during the early and middle Holocene.

During the late Holocene, there was a reduction of mangrove vegetation in the interior of Marajó, and the contribution of freshwater organic matter was greater than during the early and middle Holocene. The decrease in marine influence probably led to a gradual migration of mangroves from the central region to the northeastern littoral, and consequently, their isolation since at least ~1,150 cal. B.P. which is probably the result of lower tidal water salinity, caused by a wet period leading to greater river discharge during the late Holocene.

As reported by this study, the use of a combination of proxies is an efficient method for establishing a relationship between changes in the estuarine salinity gradient and the depositional environment/vegetation.

Acknowledgments We thank the members of the Laboratory of Coastal Dynamic (LADIC-UFPA) and Center for Nuclear Energy in Agriculture (CENA-USP) and the students from Laboratory of Chemical-Oceanography for their support. This study was financed by FAPESPA (Project 104/2008), CNPq (Project 473635/2012-7) and FAPESP (Project 03615-5/2007). The first author holds a scholarship from CNPq (Process 202598/2011-0). The authors would also like to thank A.R. Holland (University of Massachusetts) for the English revision of this paper.

References

Absy ML, Cleef A, Fournier M, Martin L, Servant M, Sifeddine A, da Ferreira Silva M, Soubies F, Suguio K, Turcq B, Van Der Hammen TH (1991) Mise en evidence de quatre phases d'overture de la forêt dense dans le sud-est de l'Amazonie au cours des 60,000 dernieres annees. Premiere comparision avec d'autres regions tropicales. Comptes Rendus de l'Acad des Sci 312:673–678

ANA (2003) Hydrological information system. Brazilian National Water Agency. On line dataset, 14.3 MB, http://hidroweb.ana.gov.br/baixar/mapa/Bacia1.zip

Angulo RJ, Lessa GC (1997) The Brazilian sea-level curves: a critical review with emphasis on the curves from the Paranaguá and Cananéia regions. Marine Geol 140:141–166

Angulo RJ, Suguio K (1995) Re-evaluation of the Holocene sea-level maxima for the State of Paraná, Brazil. Palaeogeogr Palaeoclim Palaeoecol 113:385–393

Angulo RJ, Giannini PCF, Suguio K, Pessenda LCR (1999) Relative sea-level changes in the last 5500 years in southern Brazil (Laguna—Imbituba region, Santa Catarina State) based on vermitid ^{14}C ages. Marine Geol 159:323–339

Angulo RJ, De Souza MC, Assine ML, Pessenda LCR, Disaró ST (2008) Chronostratigraphy and radiocarbon age inversion in the Holocene regressive barrier of Paraná, southern Brazil. Marine Geol 252:111–119

Barth JAC, Veizer J, Mayer B (1998) Origin of particulate organic carbon in the upper St. Lawrence: isotopic constraints. Earth Planet Sci Lett 162:111–121

Behling H (1993) Untersuchungen zur spätpleistozänen und holozänen Vegetations-und Klimageschichte der tropischen Küstenwälder und der Araukarienwälder in Santa Catarina (Südbrasilien). Diss Bot 206, Cramer, Berlin

Behling H, Costa ML (2001) Holocene vegetational and coastal environmental changes from the Lago Crispim record in northeastern Pará State, eastern Amazonia. Rev Paleobot Palynol 114:145–155

Behling H, Hooghiemstra H (2000) Holocene Amazon rainforest–savanna dynamics and climatic implications: high-resolution pollen record from Laguna Loma Linda in eastern Colombia. J Quat Sci 15:687–695

Behling H, Cohen MCL, Lara RJ (2001) Studies on Holocene mangrove ecosystem dynamics of the Bragança Peninsula in north-eastern Pará, Brazil. Palaeogeogr Palaeoclim Palaeoecol 167:225–242

Behling H, Cohen MCL, Lara RJ (2004) Late Holocene mangrove dynamics of the Marajó Island in northern Brazil. Veget Hist Archaeobot 13:73–80

Bird ECF (1980) Mangroves and coastal morphology. Vic Nat 97:48–58

Blasco F, Saenger P, Janodet E (1996) Mangrove as indicators of coastal change. Catena 27:167–178

Bush MB (1994) Amazonian speciation: a necessarily complex model. J Biogeogr 21:5–18

Bush MB, Colinvaux PA (1988) A 7000-year pollen record from the Amazon lowlands, Ecuador. Vegetatio 76:141–154

Bush MB, Silman MR, Urrego DH (2004) 48000 years of climate and forest change from biodiversity hotspot. Science 303:827–829

Bush MB, Silman MR, Listopad CMCS (2007) A regional study of Holocene climate change and human occupation in Peruvian Amazonia. J Biogeogr 34:1,342–1,356

Cahoon DR, Lynch JC (1997) Vertical accretion and shallow subsidence in a mangrove forest of southwestern Florida, U.S.A. Mangroves and Salt Marshes 3:173–186

Camargo MG (1999) SYSGRAN for Windows: Granulometric Analyses System. Pontal do Sul, Paraná

Castro DF, Rossetti DF, Pessenda LCR (2010) Facies, $\delta^{13}C$, $\delta^{15}N$ and C/N analyses in a late Quaternary compound estuarine fill, northern Brazil and relation to sea level. Marine Geol 274:135–150

Chapman VJ (1976) Mangrove vegetation. Cramer, Vaduz

Chivas AR, Garcia A, Van der Kaars S, Couapel MJJ, Holt S, Reeves JM (2001) Sea-level and environmental changes since the last interglacial in the Gulf of Carpentaria, Australia: an overview. Quat Int 85:19–46

Coffin RB, Fry B, Peterson BJ, Wright RT (1989) Carbon isotopic compositions of estuarine bacteria. Limnol Oceanog 34:1,305–1,310

Cohen MCL (2003) Past and current mangrove dynamics on the Bragança península, northern Brasil. Dissertation, Universität Bremen

Cohen MCL, Lara RJ (2003) Temporal changes of mangrove vegetation boundaries in Amazonia: application of GIS and remote sensing techniques. Wetlands Ecol Manag 11:223–231

Cohen MCL, Behling H, Lara RJ (2005a) Amazonian mangrove dynamics during the last millennium: the relative sea-level and the little Ice Age. Rev Palaeobot Palynol 136:93–108

Cohen MCL, Souza Filho PW, Lara RL, Behling H, Angulo R (2005b) A model of Holocene mangrove development and relative sea-level changes on the Bragança Peninsula (northern Brazil). Wetlands Ecol Manag 13:433–443

Cohen MCL, Lara RJ, Smith CB, Angélica RS, Dias BS, Pequeno T (2008) Wetland dynamics of Marajó Island, northern Brazil, during the last 1000 years. Catena 76:70–77

Cohen MCL, Lara RJ, Smith CB, Matos HRS, Vedel V (2009) Impact of sea-level and climatic changes on the Amazon coastal wetlands during the late Holocene. Veget Hist Archaeobot 18:425–439

Cohen MCL, Pessenda LCR, Behling H, Rossetti DF, França MC, Guimarães JTF, Friaes Y, Smith CB (2012) Holocene palaeoenviromental history of the Amazonian mangrove belt. Quat Sci Rev 55:50–58

Colinvaux PA (1998) A new vicariance model for Amazonian endemics. Glob Ecol Biogeogr Lett 7:95–96

Colinvaux PA, De Oliveira PE, Patiño JEM (1999) Amazon pollen manual and atlas—Manual e Atlas Palinológico da Amazônia. Hardwood, Amsterdam

Collinson J, Mountney N, Thompson D (2006) Sedimentary structures (3rd edn). Terra Publishing, Harpenden

Color Munsell (2009) Munsell soil color charts, new revised edition. Macbeth Division of Kollmorgen Instruments, New Windsor

Davis MB (2000) Palynology after Y2 K—understanding the source area of pollen in sediments. Ann Rev Earth Planet Sci 28:1–18

Deines P (1980) The isotopic composition of reduced organic carbon. In: Fritz P, Fontes JC (eds) Handbook of environmental isotope geochemistry. The terrestrial environments, vol 1. Elesvier, Amsterdam, pp 329–406

Desjardins T, Filho AC, Mariotti A, Chauvel A, Girardin C (1996) Changes of the forest savanna boundary in Brazilian Amazonia during the Holocene as revealed by soil organic carbon isotope ratios. Oecologia 108:749–756

DHN (2003) Departamento de Hidrografia e Navegação (Brazil Navy). Marinha do Brasil, Rio de Janeiro

Duke NC, Pinzón ZSM, Prada MC (1997) Large-scale damage to mangrove forests following two large oil spills in Panama. Biotropica 29:2–14

Fægri K, Iversen J (1989) In: Fægri K, Kaland PE, Krzywinski K (eds) Textbook of pollen analysis, 4th edn. Wiley, Chichester

França MC (2010) Mudanças na vegetação do litoral leste da Ilha de Marajó durante o Holoceno superior. Universidade Federal do Pará, Programa de Pós-Graduação em Geologia e Geoquímica. Dissertação de Mestrado, Belém

França CF, Sousa Filho PWM (2006) Compartimentação morfológica da margem leste da ilha de Marajó: zona costeira dos municípios de Soure e Salvaterra—Estado do Pará. Revista Brasileira de Geomorfologia 1:33–42

França M, Francisquini MI, Cohen MCL, Pessenda LCR, Rosseti DF, Guimarães J, Smith CB (2012) The last mangroves of Marajó Island—Eastern Amazon: impact of climate and/or relative sea-level changes. Rev Palaeobot Palynol 187:50–65

Freitas HA, Pessenda LCR, Aravena R, Gouveia SEM, Ribeiro AS, Boulet R (2001) Late Quaternary vegetation dynamics in the

southern Amazon basin inferred from carbon isotopes in soil organic matter. Quat Res 55:39–46
Fu R, Dickinson RE, Chen M, Wang H (2001) How do tropical sea surface temperatures influence the seasonal distribution of precipitation in the equatorial Amazon? J Climate 14:4,003–4,026
Goh KM (2006) Removal of contaminants to improve the reliability of radiocarbon dates of peats. J Soil Sci 29:340–349
Gornitz V (1991) Global coastal hazards from future sea level Rise. Palaeogeogr Palaeoclim Palaeoecol 89:379–398
Gouveia SEM, Pessenda LCR, Aravena R, Boulet R, Roveratti R, Gomes BM (1997) Dinâmica de vegetações durante o Quaternário recente no sul do Amazonas indicada pelos isótopos do carbono (^{12}C, ^{13}C e ^{14}C). Geochimica Brasiliensis 11:355–367
Grimm EC (1987) Coniss: a Fortran 77 program for stratigraphically constrained cluster analysis by the method of the incremental sum of squares. Comput Geosci 13:13–35
Guimarães JTF, Cohen MCL, França MC, Lara RJ, Behling H (2010) Model of wetland development of the Amapá coast during the late Holocene. Anais da Acad Brasileira de Ciências 82:451–465
Guimarães JTF, Cohen MCL, Pessenda LCR, França MC, Smith CB, Nogueira ACR (2012) Mid- and late-Holocene sedimentary process and palaeovegetation changes near the mouth of the Amazon River. Holocene 22:359–370
Haines EB (1976) Stable carbon isotope ratios in biota, soils and tidal water of a Georgia salt marsh. Estuar Coast Mar Sci 4:609–616
Harper CW (1984) Improved methods of facies sequence analysis. In: Walker RG (ed) Facies models. Geoscience Canada, (Reprint Series 1) Geological Association of Canada. Geological Association of Canada, Toronto, pp 11–13
Havinga AJ (1967) Palynology and pollen preservation. Rev Paleobot Palynol 2:81–98
Hermanowski B, Costa ML, Behling H (2012) Environmental changes in southeastern Amazonia during the last 25000 year revealed from a paleoecological record. Quat Res 77:138–148
Herrera LF, Urrego LE (1996) Atlas de polen de plantas útiles y cultivadas de la Amazonia colombiana (Pollen atlas of useful and cultivated plants in the Colombian Amazon region). (Estudios en la Amazonia Colombiana 11). Tropenbos-Colombia, Bogotá
Hesp PA, Dillenburg SR, Barboza EG, Clerot LCP, Tomazelli LJ, Zouain RNA (2007) Morphology of the Itapeva to Tramandai transgressive dunefield barrier system and mid to late Holocene sea level change. Earth Surf Process Landforms 32:407–414
Hutchings P, Saenger P (1987) Ecology of mangroves. Queensland University Press, St. Lucia
Lamb AL, Wilson GP, Leng MJ (2006) A review of coastal palaeoclimate and relative sea-level reconstructions using δ^{13}C and C/N ratios in organic material. Earth Sci Rev 75:29–57
Lara JR, Cohen MCL (2006) Sediment porewater salinity, inundation frequency and mangrove vegetation height in Bragança, North Brazil: an ecohydrology-based empirical model. Wetlands Ecol Manag 4:349–358
Lara RJ, Cohen MCL (2009) Palaeolimnological studies and ancient maps confirm secular climate fluctuations in Amazonia. Clim Change 94:399–408
Lentz SJ (1995) The Amazon River plume during AMASSEDS: Subtidal current variability and the importance of wind forcing. J Geophys Res 100:2,377–2,390
Liebmann B, Marengo JA (2001) Interannual variability of the rainy season and rainfall in the Brazilian Amazon Basin. J Climate 14:4,308–4,318
Lima AMM, Oliveira LL, Fontinhas RL, Lima RJS (2005) Ilha de Marajó: revisão histórica, hidroclimatológica, bacias hidrográficas e propostas de gestão. Holos Environ 5:65–80
Marengo JA, Druyan LM, Hastenrath S (1993) Observational and modeling studies of Amazonia interannual climate variability. Clim Change 23:267–286
Marengo JA, Liebmann B, Kousky VE, Filizola NP, Wainer IC (2001) Onset and end of the rainy season in the Brazilian Amazon Basin. J Climate 14:833–852
Martin L, Flexor JN, Suguio K (1995) Vibrotestemunhador leve: construção, utilização e potencialidades. Revista IG-USP 16:59–66
Martin L, Suguio K, Flexor J-M, Dominguez JML, Bittencourt ACSP (1996) Quaternary sea-level history and variation in dynamics along the Central Brazilian Coast: consequences on coastal plain construction. Anais da Acad Brasileira de Ciências 68:303–354
Martinelli LA, Pessenda LCR, Espinoza E, Camargo PB, Telles EC, Cerri CC, Victoria RL, Aravena R, Richey J, Trumbore S (1996) Carbon-13 variation with depth in soils of Brazil and climate change during the Quaternary. Oecologia 106:376–381
Martinelli LA, Victoria RL, Camargo PB, Piccolo MC, Mertes L, Richey JE, Devol AH, Forsberg BR (2003) Inland variability of carbon-nitrogen concentrations and δ^{13}C in Amazon floodplain (várzea) vegetation and sediment. Hydrol Processes 17:1,419–1,430
Meyers PA (1994) Preservation of elemental and isotopic source identification of sedimentary organic matter. Chem Geol 114:289–302
Meyers PA (1997) Organic geochemical proxies of paleoceanographic, paleolimnologic and paleoclimatic processes. Org Geochem 27:213–250
Meyers PA (2003) Applications of organic geochemistry to paleolimnological reconstructions: a summary of examples from the Laurentian Great Lakes. Org Geochem 34:261–289
Miall AD (1978) Facies types and vertical profile models in braided river deposits: a summary. In: Miall AD (ed) Fluvial sedimentology. Canadian Society of Petroleum Geologists, Calgary, pp 597–604
Middelburg JJ, Nieuwenhuize J (1998) Carbon and nitrogen stable isotopes in suspended matter and sediments from the Schelde Estuary. Marine Chem 60:217–225
Miranda MCC, Rossetti DF, Pessenda LCR (2009) Quaternary paleoenvironments and relative sea-level changes in Marajó Island (Northern Brazil): facies, δ^{13}C, δ^{15}N and C/N. Palaeogeogr Palaeoclim Palaeoecol 282:19–31
Nobre P, Shukla J (1996) Variations of sea surface temperature, wind stress, and rainfall over the Tropical Atlantic and South America. J Climate 9:2464–2479
Pessenda LCR, Camargo PB (1991) Datação radiocarbônica de amostras de interesse arqueológico e geológico por espectrometria de cintilação líquida de baixo nível de radiação de fundo. Quim Nova 14:98–103
Pessenda LCR, Valencia EPE, Martinelli LA (1996) ^{14}C measurements in tropical soil developed on basic rocks. Radiocarbon 38:203–208
Pessenda LCR, Gomes BM, Aravena R, Ribeiro AS, Boulet R, Gouveia SEM (1998a) The carbon isotope record in soils along a forest-cerrado ecosystem transect: implications for vegetation changes in the Rondonia state, southwestern Brazilian Amazon region. Holocene 8:631–635
Pessenda LCR, Gouveia SEM, Aravena R, Gomes BM, Boulet R, Ribeiro AS (1998b) ^{14}C dating and stable carbon isotopes of soil organic matter in forest savanna boundary areas in the southern Brazilian Amazon region. Radiocarbon 40:1,013–1,022
Pessenda LCR, Boulet R, Aravena R, Rosolen V, Gouveia SEM, Ribeiro AS, Lamotte M (2001) Origin and dynamics of soil organic matter and vegetation changes during the Holocene in a forest-savanna transition zone, Brazilian Amazon region. Holocene 11:250–254
Pessenda LCR, Ribeiro AS, Gouveia SEM, Aravena R, Boulet R, Bendassoli JA (2004) Vegetation dynamics during the late Pleistocene in the Barreirinhas region, Maranhão State, northeastern Brazil, based on carbon isotopes in soil organic mater. Quat Res 62:183–193
Pessenda LCR, Gouveia SEM, De Oliveira PE, Aravena R (2010) Late Pleistocene and Holocene vegetation changes in

northeastern Brazil determined from carbon isotopes and charcoal records in soils. Palaeogeogr Palaeoclim Palaeoecol 297:597–608

Peterson BJ, Fry B, Hullar M, Saupe S, Wright R (1994) The distribution and stable carbon isotope composition of dissolved organic carbon in estuaries. Estuaries 17:111–121

Raymond PA, Bauer JE (2001) Use of ^{14}C and ^{13}C natural abundances for evaluating riverine, estuarine, and coastal DOC and POC sources and cycling: a review and synthesis. Org Geochem 32:469–485

Reimer PJ, Baillie MGL, Bard E, Bayliss A, Beck JW, Bertrand C, Blackwell PG, Buck CE, Burr G, Cutler KB, Damon PE, Edwards RL, Fairbanks RG, Friedrich M, Guilderson TP, Hughen KA, Kromer B, McCormac FG, Manning S, Ramsey CB, Reimer RW, Remmele S, Southon JR, Stuiver M, Talamo S, Taylor FW, Van der Plicht J, Weyhenmeyer CE (2004) INTCAL04 terrestrial radiocarbon age calibration, 0–26 cal. kyear B.P. Radiocarbon 46:1,029–1,058

Reimer PJ, Baillie MGL, Bard E, Bayliss A, Beck JW, Blackwell PG, Bronk Ramsey C, Buck CE, Burr GS, Edwards RL, Friedrich M, Grootes PM, Guilderson TP, Hajdas I, Heaton TJ, Hogg AG, Hughen KA, Kaiser KF, Kromer B, Mccormac FG, Manning SW, Reimer RW, Richards DA, Southon JR, Talamo S, Turney CSM, Van der Plicht J, Weyhenmeyer CE (2009) IntCal09 and Marine09 radiocarbon age calibration curves, 0–50000 years cal. B.P. Radiocarbon 51:1,111–1,150

Rosario RP, Bezerra MOM, Vinzon SB (2009) Dynamics of the saline front in the northern Channel of the Amazon River—influence of fluvial flow and tidal range (Brazil). J Coast Res 2:503–514

Rossetti DF, Goes AM, Valeriano MM, Miranda MCC (2007) Quaternary tectonics in a passive margin: marajó Island, northern Brazil. J Quat Sci 22:1–15

Rossetti DF, Valeriano MM, Goes AM, Thales M (2008) Palaeodrainage on Marajó Island, northern Brasil, in relation to Holocene relative sea-level dynamics. Holocene 18:1–12

Rossetti DF, Souza LSB, Prado R, Elis VR (2012) Neotectonics in the northern equatorial Brazilian margin. J South American Earth Sci 37:175–190

Roubik DW, Moreno JE (1991) Pollen and Spores of Barro Colorado Island, vol 36. Missouri Botanical Garden, St. Louis

Rull V, Vegas-Vilarrùbia T, Espinoza NP (1999) Palynological record an early-mid Holocene mangrove in eastern Venezuela: implications for sea-level rise and disturbance history. J Coast Res 15:496–504

Santos MLS, Medeiros C, Muniz K, Feitosa FAN, Schwamborn R, Macedo SJ (2008) Influence of the Amazon and Pará Rivers on water composition and phytoplankton biomass on the adjacent shelf. J Coast Res 24:585–593

Schidlowski M, Hayes JM, Kaplan IR (1983) Isotopic inferences of ancient biochemistries: carbon, sulphur, hydrogen and nitrogen. In: Scholf JW (ed) Earth's earliest biosphere, its origin and evolution. Princeton University Press, Princeton, pp 149–186

Semeniuk V (1994) Predicting the effect of sea-level rise on mangroves in northwestern Australia. J Coast Res 10:1,050–1,076

Sifeddine A, Bertrand P, Fournier M, Martin L, Servant M, Soubiès F, Suguio K, Turcq B (1994) La sédimentation organique lacustre en milieu tropical humide (Carajás, Amazonie orientale, Brésil): relation avec les changements climatiques au cours des 60,000 dernières années. Bull de La Société Geologique de France 165:613–621

Sifeddine A, Marint L, Turcq B, Volkmer-Ribeiro C, Soubiès F, Cordeiro RC, Suguio K (2001) Variations of the Amazonian rainforest environment: a sedimentological record covering 30000 years. Palaeogeogr Palaeoclim Palaeoecol 168:221–235

Smith CB, Cohen MCL, Pessenda LCR, França M, Guimarães JTF, Rossetti DF (2011) Holocene coastal vegetation changes at the mouth of the Amazon River. Rev Palaeobot Palynol 168:21–30

Smith CB, Cohen MCL, Pessenda LCR, França MC, Guimarães JTF (2012) Holocenic proxies of sedimentary organic matter and the evolution of Lake Arari-Northern Brazil. Catena 90:26–38

Souza Filho PWM, Martins ESF, Costa FR (2006) Using mangroves as a geological indicator of coastal changes in the Bragança macrotidal flat, Brazilian Amazon: a remote sensing data approach. Ocean Coast Manag 49:462–475

Spenceley AP (1982) Sedimentation patterns in a mangal on Magnetic Island near Townsville, North Queensland, Australia. Singap. J Trop Geogr 3:100–107

Stockmarr J (1971) Tablets with spores used in absolute pollen analysis. Pollen Spores 13:614–621

Stuiver M, Reimer P, Braziunas TF (1998) High precision radiocarbon age calibration for terrestrial and marine samples. Radiocarbon 40:1,127–1,151

Suguio K, Martin L, Bittencourt ACSP, Dominguez JML, Flexor JM, Azevedo AEG (1985) Flutuações do Nível do Mar durante o Quaternário Superior ao longo do Litoral Brasileiro e suas Implicações na Sedimentação Costeira. Revista Brasileira de Geociência 15:273–286

Sukigara C, Saino T (2005) Temporal variations of $\delta^{13}C$ and $\delta^{15}N$ in organic particles collected by a sediment trap at time-series station off the Tokyo Bay. Continental Shelf Res 25:1,749–1,767

Thornton SF, McManus J (1994) Applications of organic carbon and nitrogen stable isotope and C/N ratios as source indicators of organic matter provenance in estuarine systems: evidence from the Tay Estuary, Scotland. Estuarine, Coastal Shelf Sci 38:219–233

Tomazelli LJ (1990) Contribuicão ao Estudo dos Sistemas Deposicionais Holocênicos do Nordeste da Província Costeira do Rio Grande do Sul, com Ênfase no Sistema Eólico, Doctoral Thesis (Tese de Doutorado). Universidade Federal do Rio Grande do Sul, Porto Alegre

Tyson RV (1995) Sedimentary organic matter: organic facies and palynofacies. Chapman and Hall, London

Vedel V, Behling H, Cohen MCL, Lara RJ (2006) Holocene mangrove dynamics and sea-level changes in Taperebal, northeastern Pará State, northern Brazil. Veget Hist Archaeobot 15:115–123

Vinzon BS, Vilela CPX, Pereira LCC (2008) Processos físicos na Plataforma Continental Amazônica. Relatório-Técnico, Potenciais Impactos Ambientais do Transporte de Petróleo e Derivados na Zona Costeira Amazônico. Petrobrás, Brasil

Walker RG (1992) Facies, facies models and modern stratigrahic concepts. In: Walker RG, James NP (eds) Facies models—response to sea level change. Geological Association of Canada, Ontario, pp 1–14

Weng C, Bush MB, Athens JS (2002) Two histories of climate change and hydrarch succession in Ecuadorian Amazonia. Rev Palaeobot Palynol 120:73–90

Weng C, Bush MB, Silman MR (2004) An elevation transect of modern pollen spectra from Amazonia to the high Andes, Peru. J Trop Ecol 20:113–124

Wentworth CK (1922) A scale of grade and class terms for clastic sediments. J Geol 30:377–392

Wolanski E, Mazda Y, King B, Gay S (1990) Dynamics, flushing and trapping in Hinchinbrook channel, a giant mangrove swamp, Australia. Estuarine, Coastal Shelf Sci 31:555–579

Woodroffe CD, Chappell J, Thom BG, Wallensky E (1989) Depositional model of a macrotidal estuary and floodplains, South Alligator River, Northern Australia. Sedimentology 36:737–756

Xu Q, Tian F, Bunting MJ, Li Y, Ding W, Cao X, He Z (2012) Pollen source areas of lakes with inflowing rivers: modern pollen influx data from Lake Baiyangdian, China. Quat Sci Rev 37:81–91